Skin marker-based versus bone morphology-based coordinate systems of the hindfoot and forefoot

Chantal M Hulshof [a,b,c,d,*], Wouter Schallig [a,b,c,d,*], Josien C van den Noort [b,d], Geert J Streekstra [b,f], Roeland P Kleipool [e], Johannes GG Dobbe [f], Mario Maas [b,d], Jaap Harlaar [c,g,h], Marjolein M van der Krogt [a,c,d]

[a] Department of Rehabilitation Medicine, Amsterdam UMC, University of Amsterdam, Meibergdreef 9 1105 AZ, Amsterdam, the Netherlands
[b] Department of Radiology and Nuclear Medicine, Amsterdam UMC, University of Amsterdam, Meibergdreef 9 1105 AZ, Amsterdam, the Netherlands
[c] Department of Rehabilitation Medicine, Amsterdam UMC, Vrije Universiteit Amsterdam, De Boelelaan 1118 1081 HZ, Amsterdam, the Netherlands
[d] Amsterdam Movement Sciences, Rehabilitation & Development, Amsterdam, the Netherlands
[e] Department of Medical Biology, Amsterdam UMC, University of Amsterdam, Meibergdreef 9 1105 AZ, Amsterdam, the Netherlands
[f] Department of Biomedical Engineering and Physics, Amsterdam UMC, University of Amsterdam, Meibergdreef 9 1105 AZ, Amsterdam, the Netherlands
[g] Department of Biomechanical Engineering, Delft University of Technology, Mekelweg 2 2628 CD, Delft, the Netherlands
[h] Department of Orthopedics & Sports Medicine, Erasmus MC, Doctor Molewaterplein 40 3015 GD, Rotterdam, the Netherlands

ARTICLE INFO

ABSTRACT

Segment coordinate systems (CSs) of marker-based multi-segment foot models are used to measure foot kinematics, however their relationship to the underlying bony anatomy is barely studied. The aim of this study was to compare marker-based CSs (MCSs) with bone morphology-based CSs (BCSs) for the hindfoot and forefoot. Markers were placed on the right foot of fifteen healthy adults according to the Oxford, Rizzoli and Amsterdam Foot Model (OFM, RFM and AFM, respectively). A CT scan was made while the foot was loaded in a simulated weight-bearing device. BCSs were based on axes of inertia. The orientation difference between BCSs and MCSs was quantified in helical and 3D Euler angles. To determine whether the marker models were able to capture inter-subject variability in bone poses, linear regressions were performed. Compared to the hindfoot BCS, all MCSs were more toward plantar flexion and internal rotation, and RFM was also oriented toward more inversion. Compared to the forefoot BCS, OFM and RFM were oriented more toward dorsal and plantar flexion, respectively, and internal rotation, while AFM was not statistically different in the sagittal and transverse plane. In the frontal plane, OFM was more toward eversion and RFM and AFM more toward inversion compared to BCS. Inter-subject bone pose variability was captured with RFM and AFM in most planes of the hindfoot and forefoot, while this variability was not captured by OFM. When interpreting multi-segment foot model data it is important to realize that MCSs and BCSs do not always align.

1. Introduction

Marker-based multi-segment foot models are often used in many different clinical populations to quantify foot kinematics during gait (Leardini et al., 2019). The Oxford Foot Model (OFM) (Stebbins et al., 2006) and Rizzoli Foot Model (RFM) (Leardini et al., 2007) are among the most frequently used multi-segment foot models both in research and practical care (Leardini and Caravaggi, 2017; Leardini et al., 2019). Recently, the Amsterdam Foot Model (AFM) has been developed, which is a follow-up of OFM and RFM. AFM is a clinically informed multi-

segment foot model that is specifically based on minimizing previously shown measurement errors (Schallig et al., 2022). All these models use skin-mounted markers placed on bony landmarks to define anatomical segment coordinate systems (CSs) for the hindfoot and forefoot that represent the underlying bone or groups of bones and aim for clinically relevant outcome measures. However, anatomical segment CSs differ considerably between multi-segment foot models, due to differences in marker location and definitions to determine the anatomical segment CSs (Schallig et al., 2020).

Preferably, marker-based CSs (MCSs) follow the underlying bony

anatomy in order to measure the bone poses and segment kinematics during standing and gait. A skewed anatomical MCS with respect to the underlying bony anatomy will result in a different distribution of measured kinematics over the three anatomical planes for the same 3D motion. Hence, it is important that the anatomical MCSs are intuitive, for example by being aligned with the bone poses. Considerable variations are present in bone morphology and relative foot bone poses between individuals (Ledoux et al., 2006; Moore et al., 2019). Therefore, it could be argued that marker models need to be able to follow the bone poses of individuals and capture these variations to allow for accurate data collection, proper data interpretation and clinical decision-making.

To our knowledge, only one study compared anatomical MCSs of the foot with their underlying bony anatomy (Zavatsky et al., 2019). This study compared the hindfoot MCS of OFM with a bone morphology-based CS (BCS) based on axes of inertia of the calcaneus and talus (Zavatsky et al., 2019). The orientation difference between the MCS and both BCSs was highly variable between subjects, particularly in the sagittal and frontal plane. Therefore, accurate protocols and thorough instruction on marker placement are paramount for new clinical gait practitioners (Zavatsky et al., 2019). Nevertheless, over the whole group they found that OFM CS was more towards plantar flexion, inversion and internal rotation relative to the calcaneal bone morphology-based CS. Generally, clinicians assume that the output of foot models represent the underlying bony anatomy. Hence, it is important that the anatomical MCSs are intuitive. However, so far, only the BCS and MCS of the hindfoot segment of OFM have been compared. A similar comparison for the forefoot segment of OFM, and hindfoot and forefoot segments of other foot models (e.g. RFM and AFM) is lacking, while this would provide insight in the anatomical accuracy of the anatomical marker CSs. For clinical practice, insights in the relation between BCSs and MCSs is important to take into account in order to facilitate clinical decision-making. Therefore, the overall aim of this study was to compare MCSs based on OFM, RFM and AFM with BCS for the hindfoot and forefoot. Specifically, we investigated 1) the orientation difference between MCSs and BCSs and 2) whether the marker models were able to capture inter-subject variability in bone poses.

2. Methods

2.1. Data collection

A detailed description of the data collection is presented in Schallig et al. (2021). The protocol was approved by the local medical ethics committee of Amsterdam UMC, location AMC, Amsterdam, the Netherlands (registration number: NL66940.018.18). Fifteen healthy subjects (8 females, age: 24.9 ± 1.8 years, height: 176.7 ± 7.5 cm, weight: 73.2 ± 12.1 kg, EU foot size: 40.9 ± 2.2 (range: 37–44)) with an asymptomatic right foot and ankle were included. Twenty-four reflective spherical skin-mounted markers (⌀9.5 mm) were placed on the right foot and ankle, according to OFM (Stebbins et al., 2006), RFM (Leardini et al., 2007) and AFM (Schallig et al., 2022). A custom-made weight-bearing simulating device (Kleipool et al., 2018) was used in a computed tomography (CT) scanner (Brilliance 64 CT scanner, Philips Medical Systems, Best, the Netherlands) to load the foot in a horizontal body position. Subjects placed their right foot in neutral position (i.e. approximately 0° ankle dorsiflexion) on a footplate containing three embedded reflective markers and extended their knee (Schallig et al., 2021b). The foot was scanned unloaded and loaded with 70 % of subjects' body weight, which is more than sufficient to simulate weight-bearing (Kang et al., 2017), and this load was measured with a digital spring balance (Type HCB200K500, KERN & SOHN GmbH, Balingen, Germany).

2.2. Data processing

CT-scans were processed with custom-made software, for details see Dobbe et al. (2019). In the unloaded neutral foot position scan, segmentations were performed of the calcaneus, five metatarsal bones, the markers on the hindfoot and forefoot segments, and the footplate markers. The unloaded scan was used for segmentation, because of the higher scan quality and wider joint spaces compared to the unloaded condition. Moreover, the registration does barely add any error in determining bone poses (Schallig et al., 2019). The segmentation process was initiated with threshold-connected region growing (Ibáñes and Schroeder, 2003), wherein a starting point was manually identified in the cortical bone. During this procedure, connected neighbouring voxels, with an intensity within a user-defined range, were automatically incorporated until the selection was considered satisfactory. Next, remaining gaps were filled and the outline closed with a binary closing operation (Carelsen et al., 2009). At this point, voxels could manually be added by using a painting brush. Subsequently, a Laplacian level-set segmentation algorithm (Ibáñes and Schroeder, 2003) refined the selection for a more accurate bone outline. The resulting segmentation was then used to generate a polygon mesh through the application of the marching cubes algorithm (Lorensen and Cline, 1987). Each point in this polygon mesh was assigned a gray level corresponding to the accompanying CT image. The segmented bones and markers were subsequently registered (i.e. matched) to the loaded scan. In the registration process, the correlation coefficient between the gray levels assigned to polygon points during segmentation and a target gray-level image was optimised using a Nelder-Mead downhill simplex optimizer algorithm (Nelder and Mead, 1965). This provided the marker and bone positions and bone orientations in the CS of the CT-scanner. For analyses, we only used the loaded neutral scan.

Next, the BCS and MCSs were constructed. No gold standard is available for the definition of BCSs in the foot (Lenz et al., 2021). Axes of inertia seem appropriate for describing the CSs of bony segments, because the first axis of inertia mimics the main axis of long bones (Ledoux et al., 2006; Woodburn et al., 2002), which often aligns with clinical perception. Furthermore, it is used previously in a comparable study (Zavatsky et al., 2019) and is an objective and reproducible method (Lenz et al., 2021). The hindfoot BCS was based on the calcaneal bone. The inertial axis in the longitudinal direction (x-axis) of the calcaneus represents the anteroposterior axis of the hindfoot BCS. However, the other two inertial axes are not towards generally accepted anatomical directions (Fig. 1a). In addition, Zavatsky et al. (2019) indicated that the hindfoot CS of OFM does not represent the whole calcaneal bone, but only the posterior tuberosity in the frontal plane. Therefore, for a better comparison, a posterior segment is clipped at 30 % (based on visual inspection of all calcanei) of the calcaneal length (Fig. 1b) so its inertial axis (largest eigen value) captures the calcaneal tuberosity orientation, which served as the temporary vertical axis. This is a temporary axis because it is not necessarily perpendicular to the anteroposterior axis of the whole calcaneal bone. The mediolateral axis (z-axis) was determined by taking the cross product of the unit vectors of the anteroposterior axis and temporary vertical axis. Finally, the final vertical axis (y-axis) was obtained by taking the cross product of the anteroposterior and mediolateral axes (Fig. 1c). The forefoot BCS was based on the five metatarsal bones. Axes of inertia were determined per metatarsal bone. We averaged the anteroposterior axes (x-axis) and vertical axes (y-axis) of the five metatarsal bones. The average vertical axis served as temporary axis. Next, the mediolateral axis (z-axis) was determined by taking the cross product of the unit vectors of the average anteroposterior axes and temporary vertical axis. Finally, the final vertical axis (y-axis) was obtained by taking the cross product of the anteroposterior and mediolateral axes. The MCSs of the hindfoot and forefoot were determined according to OFM, RFM and AFM definitions (Leardini et al., 2007; Schallig et al., 2022, 2020; Stebbins et al., 2006) using custom Matlab scripts (Mathworks, California, United States, version R2022b). The footplate CS was based on the three footplate markers and extracted from the custom-made software (Dobbe et al., 2019).
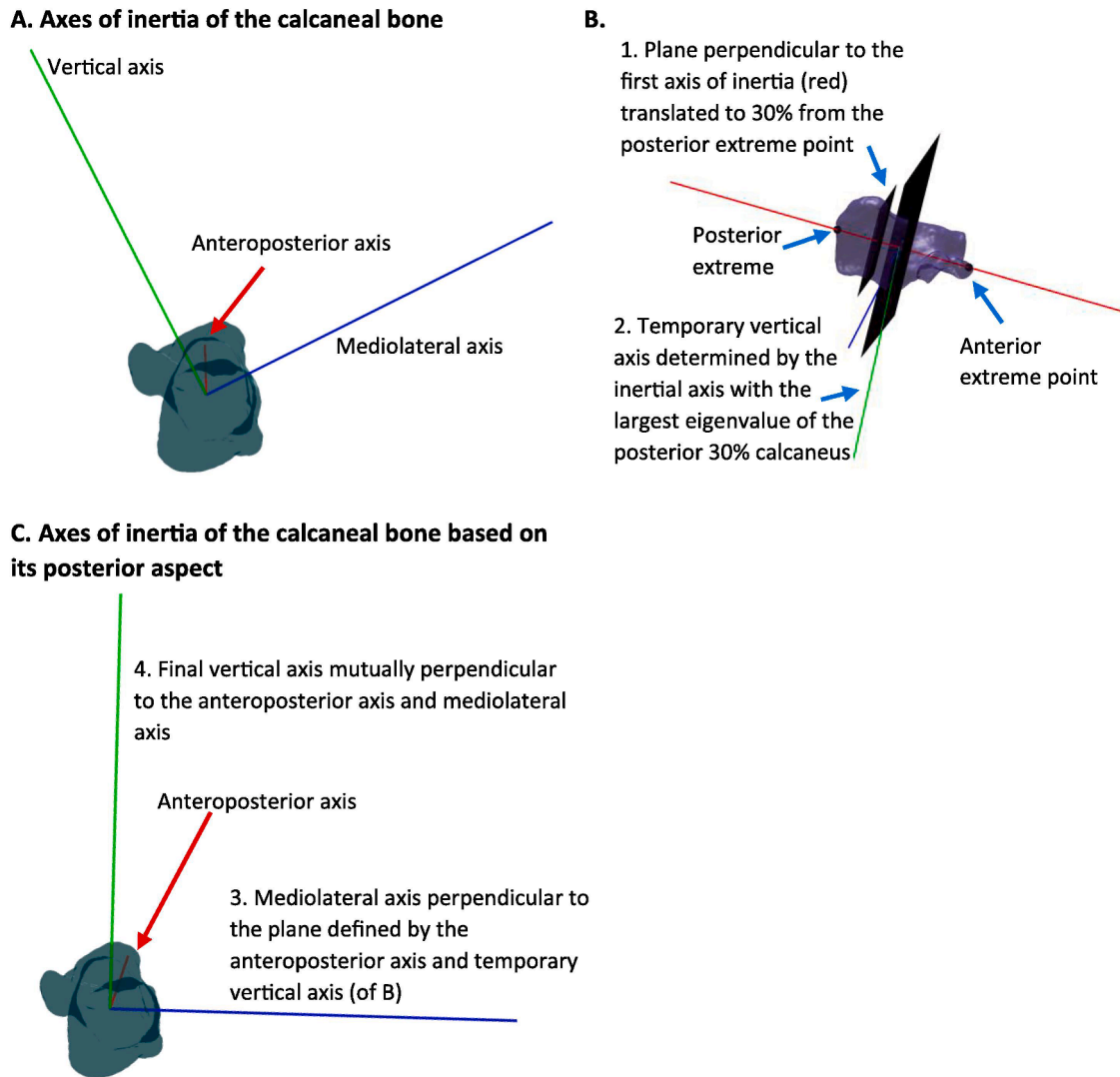
A. Axes of inertia of the calcaneal bone

Vertical axis

Anteroposterior axis

Mediolateral axis

B.

1. Plane perpendicular to the first axis of inertia (red) translated to 30% from the posterior extreme point

Posterior extreme

2. Temporary vertical axis determined by the inertial axis with the largest eigenvalue of the posterior 30% calcaneus

Anterior extreme point

C. Axes of inertia of the calcaneal bone based on its posterior aspect

4. Final vertical axis mutually perpendicular to the anteroposterior axis and mediolateral axis

Anteroposterior axis

3. Mediolateral axis perpendicular to the plane defined by the anteroposterior axis and temporary vertical axis (of B)

Fig. 1. Method to define a local coordinate system for the calcaneus. A: Axes of inertia of the calcaneal bone, with the vertical (green) and mediolateral (blue) axis not toward generally accepted anatomical directions. B: Calcaneal bone with the temporary vertical (green) axis based on the axes of inertia of the posterior 30% calcaneus. C: Calcaneal bone with the vertical (green) and mediolateral (blue) axis toward accepted anatomical directions. (For interpretation of the references to colour in this figure legend, the reader is referred to the web version of this article.)

2.3. Data analysis

Data analysis were performed using Matlab. First, we determined the rotation matrix that described the orientation of each MCS and BCS relative to the footplate ($^{Footplate}R_{BCS/MCS}$). The footplate CS ($^{Global}R_{Footplate}$) was used as reference, because we had a standard foot placement on the footplate. We determined the rotation matrix of the BCS ($^{Global}R_{BCS}$) and the MCS ($^{Global}R_{MCS}$) relative to the footplate CS for the neutral loaded scan (similar to Zavatsky et al. (2019)) (Eq. (1)).

$$\left[^{Footplate}R_{BCS/MCS} \right] = \left[^{Global}R_{Footplate} \right]^{-1} * \left[^{Global}R_{BCS/MCS} \right] \qquad (1)$$

To obtain the orientation differences in Euler angles for both the hindfoot and forefoot relative to the footplate, we decomposed the rotation matrices ($^{Footplate}R_{BCS/MCS}$) according to Grood and Suntay (1983). The first rotation was in the sagittal plane around the

mediolateral (z) axis of the BCS. The second rotation was in the frontal plane around the floating anteroposterior (x) axis and the last rotation was in the transverse plane around the vertical (y) axis of the distal segment. Orientation differences of MCSs and BCSs relative to the footplate were also quantified as helical rotation angle (φ) to have a single difference measure independent of decomposition of rotation matrices. Hence we converted the rotation matrices ($^{Footplate}R_{BCS/MCS}$) into a quaternion, and used the first dimension (quaternion$_0$) to determine the helical rotation angle (φ) according to Spring (1986) (Eq. (2)).

$$\varphi = 2 * cos^{-1}(quaternion_0) \qquad (2)$$

2.4. Statistical analysis

To compare orientation differences in helical rotation and Euler angles between MCSs and BCSs, we used one-way ANOVAs with post

hoc paired t-tests with Bonferonni correction. In order to analyze whether marker models were able to capture inter-subject variability in bone poses in 3D, we used linear regression analyses between MCSs relative to the footplate and BCSs relative to the footplate. A flatter slope than the identity line indicates that the MCS measured less variation between subjects compared to the BCS and vice versa for a steeper slope. All statistical analyses were performed using Matlab.

3. Results

3.1. Orientation difference

BCSs and MCSs of the hindfoot and forefoot of a representative subject are displayed in Fig. 2 to show a typical example of the orientation of the CSs relative to each other. For the hindfoot, all MCSs had a different helical rotation angle compared to the BCS (OFM: mean difference (Δ) 13°, RFM: Δ6°, AFM: Δ13°; p < 0.001, Fig. 3). In the sagittal plane, all MCSs were more toward plantar flexion compared to the BCS (OFM: Δ18°, RFM: Δ28°, AFM: Δ14°; p < 0.001). In the frontal plane, OFM and AFM MCSs were not significantly different from the BCS (p ≥ 0.5), while RFM MCS was in 7° more inversion compared to the BCS (p < 0.001). In the transverse plane, all MCSs were more towards internal rotation compared to the BCS (OFM: Δ8°, RFM: Δ5°, AFM: Δ5°; p < 0.001, Fig. 3).

For the forefoot, OFM and RFM MCSs had a different helical rotation angle compared to BCS (OFM: Δ8°, RFM: Δ31°; p < 0.001, Fig. 4), while the AFM MCS helical rotation angle was not significantly different (p = 0.376). In the sagittal plane, OFM and RFM MCSs were more toward dorsal and plantar flexion compared to the BCS (OFM: Δ28°, RFM: Δ31°; p < 0.001), respectively, while the AFM MCS was not significantly different from BCS (p = 0.999). In the frontal plane, the OFM MCS was more towards eversion and the RFM and AFM MCSs were more towards inversion compared to the BCS (OFM: Δ5°, RFM: Δ10°, AFM: Δ5°; p ≤

0.003). In the transverse plane, OFM and RFM MCSs were more towards internal rotation compared to the BCS (OFM: Δ7°, RFM: Δ8°; p < 0.001), while AFM MCS was not significantly different from the forefoot BCS (p = 1.000, Fig. 4).

3.2. Inter-subject variability

For the hindfoot, we found no significant association between OFM MCS and BCS in all planes (Fig. 5). For RFM and AFM MCSs there was a significant association in the sagittal and transverse plane, while there was no significant association in the frontal plane. In the sagittal plane, the coefficient of RFM and AFM MCSs was 0.48 and 0.56, and they explained 0.307 and 0.519 of the inter-subject variation respectively (Fig. 5). In the transverse plane, the coefficient of RFM and AFM MCSs was 0.64 and 0.62, and they explained 0.444 and 0.440 of the inter-subject variation respectively.

For the forefoot, we found no significant association between OFM MCS and BCS in all planes (Fig. 6). For RFM MCS there was a significant association with BCS in the sagittal and frontal plane, while for AFM MCS there was a significant association in all planes. In the sagittal plane, the coefficient of RFM and AFM MCSs was 1.31 and 0.77, and they explained 0.552 and 0.654 of the inter-subject variation respectively (Fig. 6). In the frontal plane, RFM and AFM MCSs coefficients were 0.40 and 0.44, and they explained 0.325 and 0.565 of the inter-subject variation respectively. In the transverse plane, the coefficient of AFM was 0.79 and it explained 0.793 of the inter-subject variation.

4. Discussion

This study provides insight in the comparison between BCSs, as defined by axes of inertia, and MCSs of two of the most frequently used multi-segment foot models (i.e. OFM and RFM) as well as a recently developed multi-segment foot model (i.e. AFM) for both the hindfoot and forefoot. Our main findings were that in the hindfoot all MCSs were oriented significantly different compared to BCS. In the forefoot, OFM and RFM MCSs had significantly different orientations compared to BCS, while AFM MCS only differed significantly in the frontal plane. Some of the inter-subject variability was captured by RFM and AFM MCSs in the hindfoot and forefoot bone poses. OFM MCS was not able to capture inter-subject variability in the hindfoot and forefoot bone poses.

The vertical axis of our hindfoot BCS followed the posterior aspect of the calcaneus, aligning with marker models and clinical observations of the calcaneal orientation in the frontal plane (i.e. varus/valgus) (Zavatsky et al., 2019). In addition, we replicated the method of Zavatsky et al. (2019) and determined the hindfoot BCS based on axes of inertia of the entire calcaneus. For both studies, OFM MCS was oriented more toward plantar flexion, inversion and internal rotation relative to the hindfoot BCS (Appendix A). However, our method based on the posterior aspect did measure the same orientation in the frontal plane as the marker models. Orientation differences were largest in the sagittal plane, suggesting that mainly the calcaneal pitch is not represented well by the marker models. This could be expected based on the marker locations of the models, which are not related to the calcaneal pitch. (Leardini et al., 2007; Schallig et al., 2022, 2020; Stebbins et al., 2006).

Orientation differences between MCSs and BCSs of the forefoot have, to our knowledge, not yet been described in literature. Differences were again largest in the sagittal plane. These orientation differences can be explained by the definitions of the anatomical CSs of the models (Leardini et al., 2007; Schallig et al., 2022, 2020; Stebbins et al., 2006). In healthy feet the inclination angle of metatarsal bones with respect to the floor is around 25° according to literature (Cheung et al., 2018) and 18° (SD: 5°) in our dataset. OFM MCSs during total foot contact are roughly aligned to the floor, hence the forefoot is measured in more dorsal flexion (Stebbins et al., 2006). RFM MCS defines the anterior axis of the forefoot from a marker on top of the 2nd metatarsal basis to the midpoint between the 1st and 5th metatarsal heads, hence the forefoot is
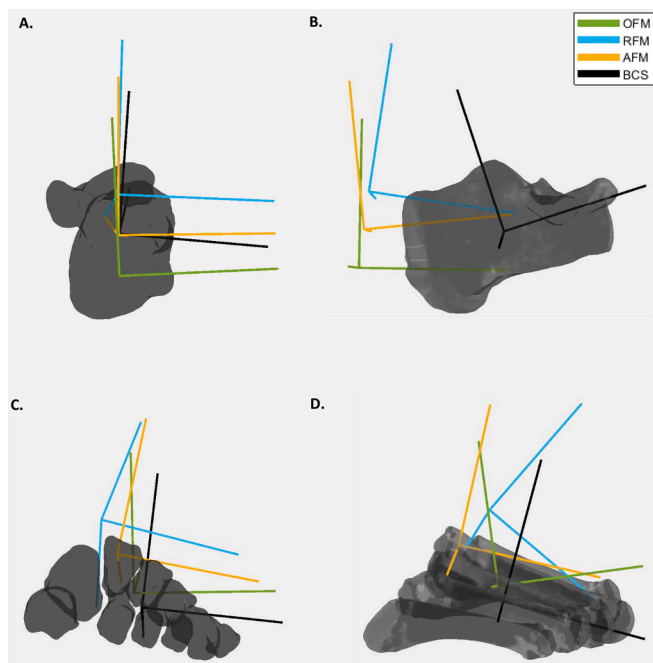

Fig. 2. Bone and marker coordinate systems of the hindfoot and forefoot of a representative subject. A. back view hindfoot, B. medial view hindfoot, C. back view forefoot, D. medial view forefoot. (OFM = Oxford foot model, RFM = Rizzoli foot model, AFM = Amsterdam foot model, BCS = bone coordinate system).
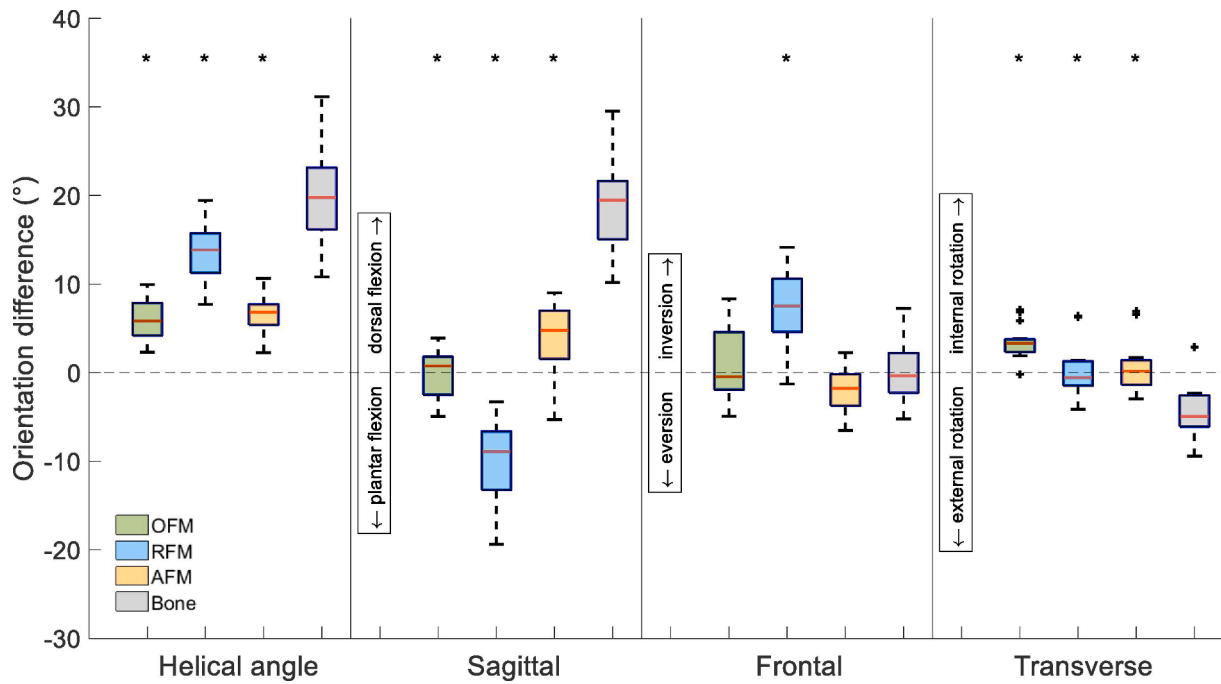
Fig. 3. Hindfoot mean orientation difference between marker-based and bone-embedded CSs and the footplate CS in neutral loaded foot position in degrees for OFM, RFM, AFM and bone coordinate systems. * = significantly different from the hindfoot BCS (p < 0.001). (OFM = Oxford foot model, RFM = Rizzoli foot model, AFM = Amsterdam foot model, CS = coordinate system).
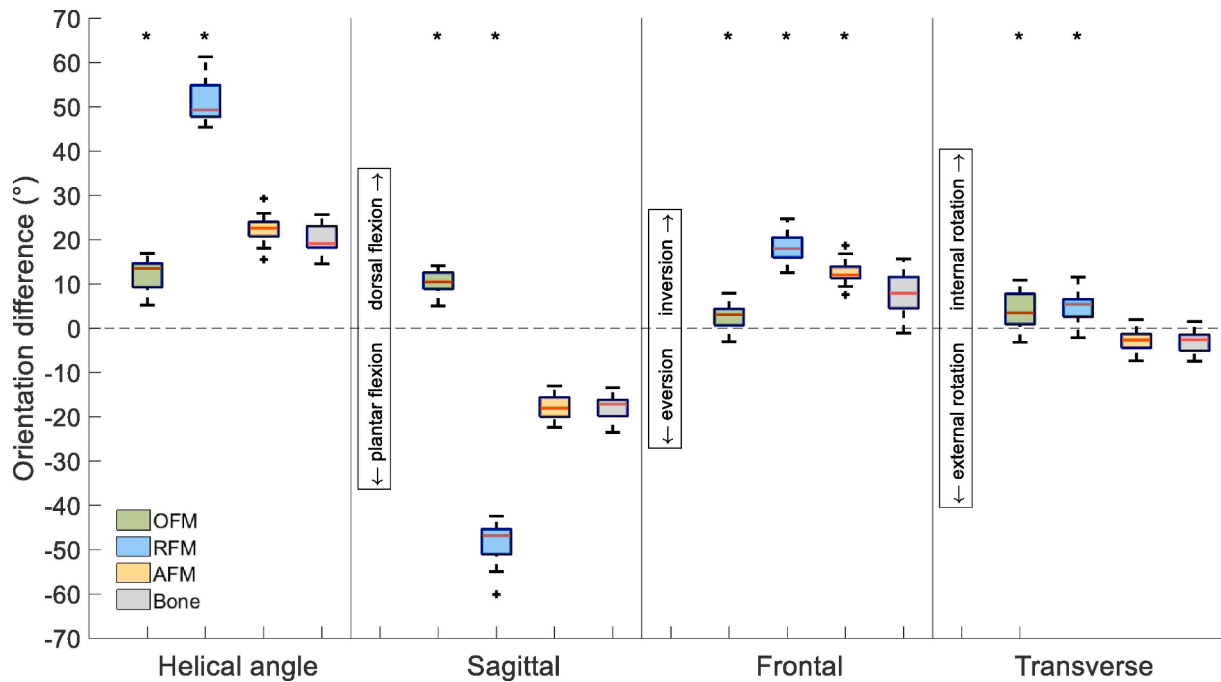

Fig. 4. Forefoot mean orientation difference between marker-based and bone-embedded CSs and the footplate CS in neutral loaded foot position in degrees for OFM, RFM, AFM and bone coordinate systems. * = significantly different from the forefoot BCS (p ≤ 0.003). (OFM = Oxford foot model, RFM = Rizzoli foot model, AFM = Amsterdam foot model, CS = coordinate system).

measured in more plantar flexion (Fig. 2) (Leardini et al., 2007). AFM MCS uses the midpoints between markers at the metatarsal bases and the midpoints between the metatarsal heads and therefore closely follows the inclination angle of metatarsal bones (Schallig et al., 2022). This explains why the forefoot segments of OFM and RFM MCSs were oriented differently compared to the forefoot BCS, while AFM MCS was oriented similar as the forefoot BCS.

An orientation difference between a MCS and the corresponding BCS does not have to be an issue during gait analysis and its interpretation, as long as the models are sensitive in detecting differences in segment orientation across subjects and across the gait cycle. The results show that RFM and AFM MCSs seem able to capture some of the inter-subject variability in bone orientation of the hindfoot and forefoot. However, the presented regression coefficients are not equal to one. A coefficient
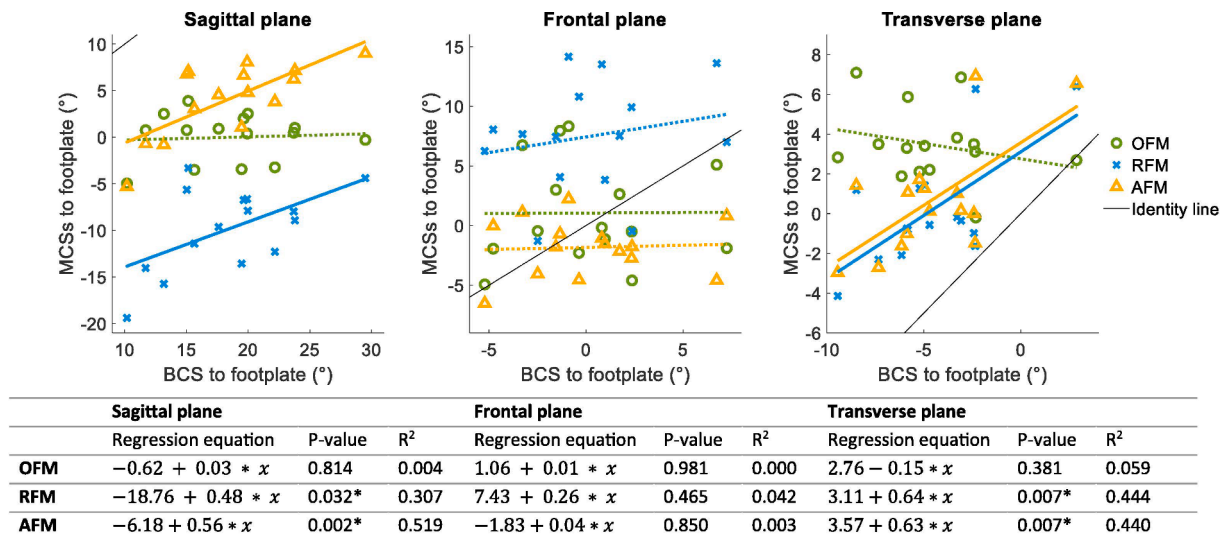
Fig. 5. Linear regression equations and explained variances between OFM, RFM and AFM marker-based CSs and the bone-embedded CS for the hindfoot. * = significant association, depicted as a solid line. Non-significant associations are depicted as a dotted line. (MCSs = marker-based CSs, BCSs = bone-embedded CSs, OFM = Oxford Foot Model, RFM = Rizzoli Foot Model, AFM = Amsterdam Foot Model).

	Sagittal plane			Frontal plane			Transverse plane		
	Regression equation	P-value	R^2	Regression equation	P-value	R^2	Regression equation	P-value	R^2
OFM	$-0.62 + 0.03 * x$	0.814	0.004	$1.06 + 0.01 * x$	0.981	0.000	$2.76 - 0.15 * x$	0.381	0.059
RFM	$-18.76 + 0.48 * x$	0.032*	0.307	$7.43 + 0.26 * x$	0.465	0.042	$3.11 + 0.64 * x$	0.007*	0.444
AFM	$-6.18 + 0.56 * x$	0.002*	0.519	$-1.83 + 0.04 * x$	0.850	0.003	$3.57 + 0.63 * x$	0.007*	0.440

Fig. 6. Linear regression equations and explained variances between OFM, RFM and AFM marker-based CSs and the bone-embedded CS for the forefoot. * = significant association, depicted as a solid line. Non-significant associations are depicted as a dotted line. (MCSs = marker-based CSs, BCSs = bone-embedded CSs, OFM = Oxford Foot Model, RFM = Rizzoli Foot Model, AFM = Amsterdam Foot Model).
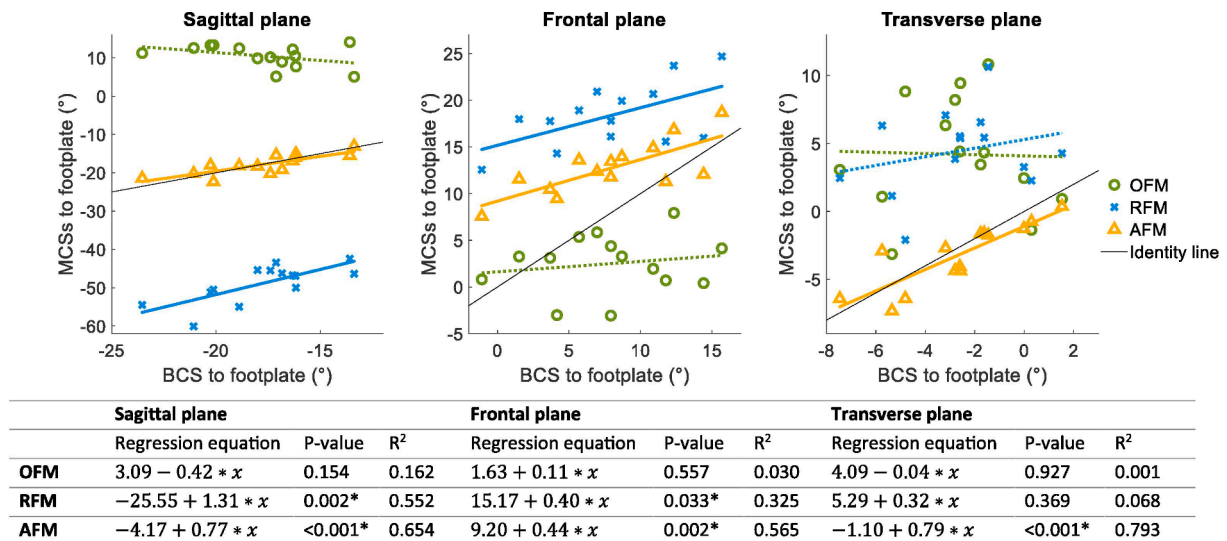
	Sagittal plane			Frontal plane			Transverse plane		
	Regression equation	P-value	R^2	Regression equation	P-value	R^2	Regression equation	P-value	R^2
OFM	$3.09 - 0.42 * x$	0.154	0.162	$1.63 + 0.11 * x$	0.557	0.030	$4.09 - 0.04 * x$	0.927	0.001
RFM	$-25.55 + 1.31 * x$	0.002*	0.552	$15.17 + 0.40 * x$	0.033*	0.325	$5.29 + 0.32 * x$	0.369	0.068
AFM	$-4.17 + 0.77 * x$	<0.001*	0.654	$9.20 + 0.44 * x$	0.002*	0.565	$-1.10 + 0.79 * x$	<0.001*	0.793

of one means that the exact same amount of between-subjects variability is measured in BCS and MCS. This is likely due to the fact that only a part of the bone(s) in the segment is tracked and important to realize when interpreting marker-based gait analysis. Nevertheless, RFM and AFM models do capture some of the variability, while OFM MCS is not able to capture variability at all. Likely, this is a result of OFM often aligning its CSs to the floor, while RFM and AFM use more bony landmarks to define their anatomical CSs (Leardini et al., 2007; Schallig et al., 2022, 2020; Stebbins et al., 2006). Depending on whether the clinicians would like to track roughly the foot sole or the foot bones they should choose the suitable model.

The definition of BCSs of foot segments is challenging, since no gold standard is available in literature (Lenz et al., 2021). In other parts of the body, like the femur and tibia, the long axes are more intuitively defined from joint center to joint center (Tesch, 2014). However, this method is difficult to apply to the calcaneus. Bony landmarks or geometric shapes to define the axes of the calcaneus have been used (Parra et al., 2012;

Yamaguchi et al., 2009), but these methods are susceptible to inter- and intra-user variability (Brown et al., 2020; Lenz et al., 2021). Instead, the axes of inertia of foot bones in the hindfoot can be determined automatically and reliably (Brown et al., 2020). Moreover they are frequently used in literature (Goto et al., 2009; Mattingly et al., 2006; Siegler et al., 2005; Zavatsky et al., 2019), which allows for comparison between studies. Therefore, we chose to use the axes of inertia in this study, but consensus on the BCSs of the foot and ankle is needed to progress the field of foot and ankle biomechanics and make better use of upcoming imaging modalities like weight-bearing CT (Barg et al., 2018) and dual-fluoroscopy (Ye et al., 2021). Little research has been done on BCSs of the forefoot, which consists of more bones and joints. Since the axes of inertia of bones generally mimic the clinical definitions of long bone axes (Gutekunst et al., 2013), we chose to average the axes of inertia of the five metatarsal bones.

Although the output of gait analyses are generally joint angles during walking, in the current study we chose to focus on segment orientations.

Joint angles in multi-segment foot models are typically calculated by decomposing the rotation matrix from a proximal to a distal segment for example with the Grood and Suntay (1983) joint convention. Hence, orientation differences in the anatomical segment CSs do also affect the calculated joint angles. However, when calculating joint angles during gait, other factors like soft tissue artifacts play a role (Schallig et al., 2021b). Hence, we performed the comparison solely on the segment orientations to compare MCS and BCS directly.

We should address several limitations of our study. First, we only included 15 asymptomatic feet, resulting in a small range of bone poses. Especially in the frontal plane of the hindfoot all models are sensitive to marker misplacement (Schallig et al., 2021a), leading to measurement errors around 5°. Given that our small sample mostly exhibited ± 5° varus/valgus bony orientation relative to the footplate, marker models are likely not sufficiently sensitive to detect differences within this small range. Future research should investigate the sensitivity of a marker model to detect differences in a wider range of foot types including bony foot deformities. In people with foot deformities, we expect orientation differences to be in the same range of values as asymptomatic feet because markers are placed according to the bony anatomy. However, the inter-subject variability might be different due to a wider range of foot types. Second, we compared the CSs during loading in only one foot position. Investigating more foot positions would give insight in whether the orientation differences remain consistent during movement, which is important knowledge when applying these results to clinical gait analysis. However, based on the small soft tissue artefacts found in previous research (Schallig et al., 2021b), we expect no large differences in orientation difference across the gait cycle (i.e. other foot positions). Third, for foot loading we used a semi-weight-bearing device. Performing scans with actual weight bearing might be beneficial, however it has been shown that the 70 % weight bearing that was reached in this study is sufficient to simulate standing (Kang et al., 2017). Last, we only included the MCSs of three multi-segment foot models, while more than 40 have been developed (Leardini et al., 2019). However, the two most-frequently used multi-segment foot models (i.e. OFM and RFM), both in research and clinical practice, as well as a more recent follow-up model (i.e. AFM) were used in this study.

Clinically, it is important to realize that MCSs are different from BCSs when interpreting data from multi-segment foot models. The orientation differences between the two CSs may lead to motions being expressed in different planes. These orientation differences can be corrected for by rotating the MCSs with angular values from radiographs or CT-scans, as optionally done in e.g. the Milwaukee and mSHCG foot models (Kidder et al., 2007; Saraswat et al., 2012). This allows for a better alignment between MCSs with their underlying bone anatomy. However, it requires imaging with radiation, which is not possible in all clinical settings and not preferred in all patient populations (e.g. children). Additionally, this study shows that multi-segment foot models which use bony landmarks for their anatomical CSs (i.e. RFM and AFM) are better able to detect inter-subject variability in bony anatomy compared to marker models that align their anatomical CSs to the floor or foot sole (i.e. OFM). In clinical practice, it is important that variations in segment orientation are detected across patients, as this reflects the differences in bone poses between patients and is taken into account in clinical decision-making. When abnormalities in patients are not properly detected, clinical decision making for certain treatments may be more difficult or even incorrect clinical decisions might be made.

5. Conclusion

Orientation differences are present between marker-based and bone morphology-based coordinate systems, leading to motions being expressed in different planes. Inter-subject variability in bone poses of the hindfoot and forefoot seem to be captured by RFM and AFM, but not by OFM. Detecting variations in segment orientation in patients is important, because it reflects differences in bone poses, which may influence clinical decision-making. Hence, when interpreting multi-segment foot model data it is important to realize that MCSs and BCSs do not always align.

CRediT authorship contribution statement

Chantal M Hulshof: Writing – original draft, Visualization, Validation, Software, Methodology, Investigation, Formal analysis, Data curation. **Wouter Schallig:** Writing – original draft, Visualization, Validation, Supervision, Software, Resources, Project administration, Methodology, Investigation, Formal analysis, Data curation, Conceptualization. **Josien C van den Noort:** Writing – review & editing, Validation, Supervision, Resources, Project administration, Methodology, Funding acquisition, Formal analysis, Conceptualization. **Geert J Streekstra:** Writing – review & editing, Validation, Supervision, Resources, Methodology, Investigation, Conceptualization. **Roeland P Kleipool:** Writing – review & editing, Resources, Methodology, Investigation, Conceptualization. **Johannes GG Dobbe:** Writing – review & editing, Supervision, Software, Resources, Methodology, Formal analysis, Conceptualization. **Mario Maas:** Writing – review & editing, Supervision, Funding acquisition, Conceptualization. **Jaap Harlaar:** Writing – review & editing, Supervision, Methodology, Funding acquisition, Formal analysis, Conceptualization. **Marjolein M van der Krogt:** Writing – review & editing, Supervision, Project administration, Methodology, Funding acquisition, Formal analysis, Conceptualization.

Declaration of competing interest

The authors declare that they have no known competing financial interests or personal relationships that could have appeared to influence the work reported in this paper.

Acknowledgement

Appendix A. Supplementary material

Supplementary data to this article can be found online at https://doi.org/10.1016/j.jbiomech.2024.112001.

References

Barg, A., Bailey, T., Richter, M., de Cesar, N.C., Lintz, F., Burssens, A., et al., 2018. Weightbearing computed tomography of the foot and ankle: emerging technology topical review. Foot Ankle Int. 39, 376–386. https://doi.org/10.1177/1071100717740330.

Brown, J.A., Gale, T., Anderst, W., 2020. An automated method for defining anatomic coordinate systems in the hindfoot. J. Biomech. 109, 1–6. https://doi.org/10.1016/j.jbiomech.2020.109951.

Carelsen, B., Jonges, R., Strackee, S.D., Maas, M., Van Kemenade, P., Grimbergen, C.A., et al., 2009. Detection of in vivo dynamic 3-D motion patterns in the wrist joint. IEEE Trans. Biomed. Eng. 56, 1236–1244. https://doi.org/10.1109/TBME.2008.2009069.

Cheung, Z.B., Myerson, M.S., Tracey, J., Vulcano, E., 2018. Weightbearing CT scan assessment of foot alignment in patients with hallux rigidus. Foot Ankle Int. 39, 67–74. https://doi.org/10.1177/1071100717732549.

Dobbe, J.G.G., De Roo, M.G.A., Visschers, J.C., Strackee, S.D., Streekstra, G.J., 2019. Evaluation of a quantitative method for carpal motion analysis using clinical 3-D and 4-D CT protocols. IEEE Trans. Med. Imaging 38, 1048–1057. https://doi.org/10.1109/TMI.2018.2877503.

Goto, A., Moritomo, H., Itohara, T., Watanabe, T., Sugamoto, K., 2009. Three-dimensional in vivo kinematics of the subtalar joint during Dorsi-plantarflexion and inversion-eversion. Foot Ankle Int. 30, 432–438. https://doi.org/10.3113/FAI.2009.0432.

Grood, E.S., Suntay, W.J., 1983. A joint coordinate system for the clinical description of three-dimensional motions: Application to the knee. J. Biomech. Eng. 105, 136–144. https://doi.org/10.1115/1.3138397.

Gutekunst, D.J., Liu, L., Ju, T., Prior, F.W., Sinacore, D.R., 2013. Reliability of clinically relevant 3D foot bone angles from quantitative computed tomography. J. Foot Ankle Res. 6, 1–8. https://doi.org/10.1186/1757-1146-6-38.

Ibáñes L, Schroeder W. The insight segmentation and registration toolkit, software guide. Kitware Inc; 2003.

Kang, D.H., Kang, C., Hwang, D.S., Song, J.H., Song, S.H., 2017. The value of axial loading three dimensional (3D) CT as a substitute for full weightbearing (standing) 3D CT: Comparison of reproducibility according to degree of load. Foot Ankle Surg. 1–6. https://doi.org/10.1016/j.fas.2017.10.014.

Kidder, S.M., Abuzzahab, F.S., Harris, G.F., Johnson, J.E., 2007. A system for the analysis of foot and ankle kinematics during gait. Foot Ankle Motion Anal. Clin. Treat. Technol. 4, 367–381. https://doi.org/10.1201/9781420005745-27.

Kleipool, R.P., Dahmen, J., Vuurberg, G., Oostra, R.-J., Blankevoort, L., Knupp, M., et al., 2018. Study on the three-dimensional orientation of the posterior facet of the subtalar joint using simulated weight-bearing CT. J. Orthop. Res. 1–30. https://doi.org/10.1002/jor.24163.

Leardini, A., Benedetti, M.G., Berti, L., Bettinelli, D., Nativo, R., Giannini, S., 2007. Rear-foot, mid-foot and fore-foot motion during the stance phase of gait. Gait Posture 25, 453–462. https://doi.org/10.1016/j.gaitpost.2006.05.017.

Leardini, A., Caravaggi, P., 2017. Kinematic foot models for instrumented gait analysis. Handb. Hum. Motion 1–24. https://doi.org/10.1007/978-3-319-30808-1.

Leardini, A.A., Caravaggi, P., Theologis, T., Stebbins, J., 2019. Multi-segment foot models and their use in clinical populations. Gait Posture. https://doi.org/10.1016/j.gaitpost.2019.01.022.

Ledoux, W.R., Rohr, E.S., Ching, R.P., Sangeorzan, B.J., 2006. Effect of foot shape on the three-dimensional position of foot bones. J. Orthop. Res. 2176–2186. https://doi.org/10.1002/jor.20262.

Lenz, A.L., Strobel, M.A., Anderson, A.M., Fial, A.V., MacWilliams, B.A., Krzak, J.J., et al., 2021. Assignment of local coordinate systems and methods to calculate tibiotalar and subtalar kinematics: A systematic review. J. Biomech. 120, 1–15. https://doi.org/10.1016/j.jbiomech.2021.110344.

Lorensen, W.E., Cline, H.E., 1987. Marching cubes: A high resolution 3D surface construction algorithm. Comput. Graph. 21, 163–169. https://doi.org/10.1145/37402.37422.

Mattingly, B., Talwalkar, V., Tylkowski, C., Stevens, D.B., Hardy, P.A., Pienkowski, D., 2006. Three-dimensional in vivo motion of adult hind foot bones. J. Biomech. 39, 726–733. https://doi.org/10.1016/j.jbiomech.2004.12.023.

Moore, E.S., Kidd, M.W., McKearney, D.A., Telfer, S., Sangeorzan, B.J., Ledoux, W.R., 2019. Hind- and midfoot bone morphology varies with foot type and sex. J. Orthop. Res. 744–759. https://doi.org/10.1002/jor.24197.

Nelder, J.A., Mead, R., 1965. A simplex method for function minimization. Comput. J. 7, 308–313. https://doi.org/10.1093/comjnl/7.4.308.

Parra, W.C.H., Chatterjee, H.J., Soligo, C., 2012. Calculating the axes of rotation for the subtalar and talocrural joints using 3D bone reconstructions. J. Biomech. 45, 1103–1107. https://doi.org/10.1016/j.jbiomech.2012.01.011.

Saraswat, P., MacWilliams, B.A., Davis, R.B., 2012. A multi-segment foot model based on anatomically registered technical coordinate systems: Method repeatability in pediatric feet. Gait Posture 35, 547–555. https://doi.org/10.1016/j.gaitpost.2011.11.022.

Schallig, W., van den Noort, J.C., Kleipool, R.P., Dobbe, J.G.G., van der Krogt, M.M., Harlaar, J., et al., 2019. Precision of determining bone pose and marker position in the foot and lower leg from computed tomography scans: How low can we go in radiation dose? Med. Eng. Phys. https://doi.org/10.1016/j.medengphy.2019.05.004.

Schallig, W., van den Noort, J.C., McCahill, J., Stebbins, J., Leardini, A., Maas, M., et al., 2020. Comparing the kinematic output of the Oxford and Rizzoli Foot Models during normal gait and voluntary pathological gait in healthy adults. Gait Posture 82, 126–132. https://doi.org/10.1016/j.gaitpost.2020.08.126.

Schallig, W., van den Noort, J.C., Maas, M., Harlaar, J., van der Krogt, M.M., 2021a. Marker placement sensitivity of the Oxford and Rizzoli foot models in adults and children. J. Biomech. 126, 1–7. https://doi.org/10.1016/j.jbiomech.2021.110629.

Schallig, W., Streekstra, G.J., Hulshof, C.M., Kleipool, R.P., Dobbe, J.G.G., Maas, M., et al., 2021b. The influence of soft tissue artifacts on multi-segment foot kinematics. J. Biomech. 120, 1–8. https://doi.org/10.1016/j.jbiomech.2021.110359.

Schallig, W., van den Noort, J.C., Piening, M., Steekstra, G., Maas, M., van der Krogt, M. M., et al., 2022. The Amsterdam Foot Model: a clinically infomed multi-segment foot model based on minimizing measurement errors in foot kinematics. Foot Ankle Res. 6, 1–15. https://doi.org/10.1186/s13047-022-00543-6.

Siegler, S., Udupa, J.K., Ringleb, S.I., Imhauser, C.W., Hirsch, B.E., Odhner, D., et al., 2005. Mechanics of the ankle and subtalar joints revealed through a 3D quasi-static stress MRI technique. J. Biomech. 38, 567–578. https://doi.org/10.1016/j.jbiomech.2004.03.036.

Spring, K.W., 1986. Euler parameters and the use of quaternion algebra in the manipulation of finite rotations: A review. Mech. Mach. Theory 21, 365–373. https://doi.org/10.1016/0094-114X(86)90084-4.

Stebbins, J., Harrington, M., Thompson, N., Zavatsky, A., Theologis, T., 2006. Repeatability of a model for measuring multi-segment foot kinematics in children. Gait Posture 23, 401–410. https://doi.org/10.1016/j.gaitpost.2005.03.002.

Tesch B. An Optimization Method for Estimating Joint Parameters of the Hip and Knee 2014.

Woodburn, J., Udupa, J.K., Hirsch, B.E., Wakefield, R.J., Helliwell, P.S., Reay, N., et al., 2002. The geometric architecture of the subtalar and midtarsal joints in rheumatoid arthritis based on magnetic resonance imaging. Arthritis Rheum 46, 3168–3177. https://doi.org/10.1002/art.10676.

Yamaguchi, S., Sasho, T., Kato, H., Kuroyanagi, Y., Banks, S.A., 2009. Ankle and subtalar kinematics during dorsiflexion-plantarflexion activities. Foot Ankle Int. 30, 361–366. https://doi.org/10.3113/FAI.2009.0361.

Ye, D., Sun, X., Zhang, C., Zhang, S., Zhang, X., Wang, S., et al., 2021. In vivo foot and ankle kinematics during activities measured by using a dual fluoroscopic imaging system: a narrative review. Front. Bioeng. Biotechnol. 9, 1–10. https://doi.org/10.3389/fbioe.2021.693806.

Zavatsky, A.B., Paik, A.M.H., Leitch, J., Kothari, A., Stebbins, J., 2019. Comparison of the hindfoot axes of a multi-segment foot model to the underlying bony anatomy. J. Biomech. 1–30. https://doi.org/10.1016/j.jbiomech.2019.06.006.